BIOCHEMISTRY
including biophysical chemistry & molecular biology

Article

pubs.acs.org/biochemistry

Concerted Protein and Nucleic Acid Conformational Changes Observed Prior to Nucleotide Incorporation in a Bacterial RNA Polymerase: Raman Crystallographic Evidence

Ioanna H. Antonopoulos,[†] Brittany A. Warner,[‡,§] and Paul R. Carey*[,†]

[†]Department of Biochemistry, Case Western Reserve University School of Medicine, Cleveland, Ohio 44106, United States

[‡]Department of Biochemistry and Molecular Biology, The Center of RNA Molecular Biology, Pennsylvania State University, University Park, Pennsylvania 16802, United States

Supporting Information

ABSTRACT: Transcription elongation requires the continuous incorporation of ribonucleotide triphosphates into a growing transcript. RNA polymerases (RNAPs) are able to processively synthesize a growing RNA chain via translocation of the RNAP enzyme along its nucleic acid template strand after each nucleotide addition cycle. In this work, a time-resolved Raman spectroscopic analysis of nucleotide addition in single crystals of the *Thermus thermophilus* elongation complex (TthEC) is reported. When [^{13}C,^{15}N]GTP (*GTP) is soaked into crystals of the TthEC, large reversible changes in the Raman spectrum that are assigned to protein and nucleic acid conformational events during a single-nucleotide incorporation are observed. The *GTP population in the TthEC crystal reaches a stable population at 37 min, while substantial and reversible protein conformational changes (mainly ascribed to changes in α-helical Raman features) maximize at approximately 50 min. At the same time, changes in nucleic acid bases and phosphodiester backbone Raman marker bands occur. Catalysis begins at approximately 65−70 min, soon after the maximal protein and DNA changes, and is monitored via the decline in a triphosphate vibrational Raman mode from *GTP. The Raman data indicate that approximately 40% of the total triphosphate population, present as *GTP, reacts in the crystal. This may suggest that a second population of noncovalently bound *GTP resides in a site distinct from the catalytic site. The data reported here are an extension of our recent work on the elongation complex (EC) of a bacterial RNAP, *Thermus thermophilus* (Tth), where Raman spectroscopy and polyacrylamide gel electrophoresis were employed to monitor incorporation and misincorporation in single TthEC crystals [Antonopoulos, I. H., et al. (2015) *Biochemistry* 54, 652−665]. Therefore, the initial study establishes the groundwork for this study. In contrast to our previous study, in which incorporation takes place very rapidly inside the crystals, the data on this single crystal exhibit a slower time regime, which allows the dissection of the structural dynamics associated with GMP incorporation within the TthEC crystal.

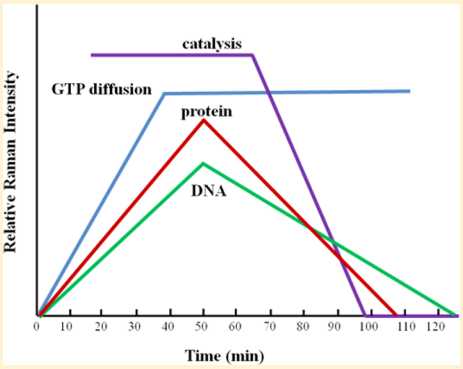

Transcription serves as a vital mechanism for regulating gene expression. RNA polymerases (RNAPs) are essential enzymes during transcription elongation as they catalyze the incorporation of nucleotide triphosphates as nucleotide monophosphates onto the 3′ end of the nascent RNA transcript. The complete process by which one nucleotide is covalently linked to the 3′ end of the nascent transcript is termed a nucleotide addition cycle. Bacterial RNAPs successively repeat this cycle at a rate of 50−100 nucleotides s^{-1} to achieve transcription elongation.[1] Despite the plethora of X-ray crystallographic studies on the transcription pathway,[2−10] the choreography of structural and catalytic events surrounding the mechanism of RNAP nucleotide incorporation remains controversial. Therefore, we set out to uniquely address these questions with a time-resolved Raman spectroscopic approach.

Here, a Raman spectroscopic study on single crystals of the bacterial *Thermus thermophilus* RNAP elongation complex (TthEC) is reported. Compared to other models, *T. thermophilus* (*Tth*) RNAP represents a simpler form of polymerase, therefore reducing the complexity of studying higher-order, eukaryotic polymerases that require additional transcription factors. *Tth* RNAP is a 380 kDa multisubunit enzyme consisting of five subunits ($\alpha_2\beta\beta'\omega$). Its architecture is often termed a crab claw (Figure 1a),[7] where the active site resides in the cleft between the pincers of enzyme subunits β and β'. In the β' subunit, two magnesium ions are in octahedral coordination with a catalytic aspartic acid triad in the active site (Figure 1b). Also in Figure 1b, the incoming NTP is stabilized by contacts with a three-helix bundle consisting of two structural motifs, the trigger loop (blue) and bridge helix (purple). The trigger loop crosses RNAP's main and secondary

Received: May 1, 2015
Revised: July 9, 2015
Published: July 29, 2015

DOI: 10.1021/acs.biochem.5b00484
Biochemistry 2015, 54, 5297−5305

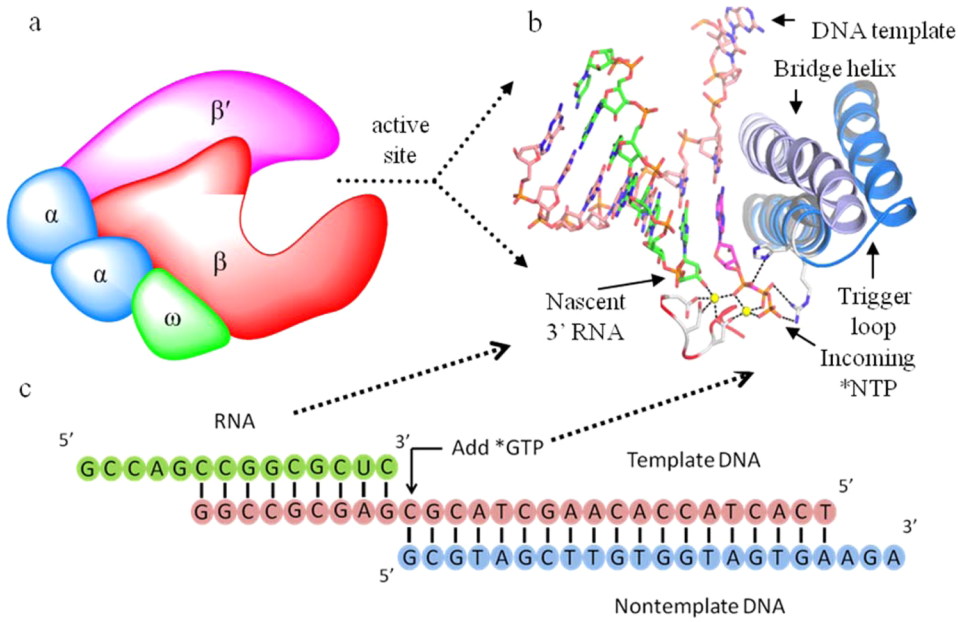

Figure 1. *T. thermophilus* RNAP elongation complex: (a) *Tth* RNAP crab claw-like architecture, (b) TthEC active site and structural motifs, and (c) nucleic acid sequences in the TthEC.

channels and can adopt open and closed conformations. When in the open or "unfolded" conformation, the trigger loop lies mostly in the main channel, with the catalytic site easily accessible via the secondary channel. When in the closed or "folded" conformation (Figure 1b), the trigger loop adopts a more ordered α-helical conformation (often called the trigger helix), forms extensive contacts with the NTP in the active site, and blocks anything from exiting or entering the catalytic site. The open and closed conformational changes in the trigger loop are also accompanied by changes in the bridge helix motif, which alternates between straight and bent conformations.[11] The TthEC crystal studied here consists of the *Tth* RNAP core enzyme, a 9 bp RNA−DNA hybrid, and a 19 bp DNA duplex as depicted previously (Figure 1c).[12]

RNAP elongation is initiated in this study by soaking *GTP into a single crystal of the TthEC. Raman microscopy is employed to monitor the nucleotidyl transfer reaction in the active site of the crystal via Raman difference spectroscopy and by using [^{13}C,^{15}N]GTP, which provides a unique Raman signature for the substrate (Figure S1). Raman difference spectra follow time-dependent structural changes observed during the *in crystallo* reaction as distinct Raman bands are assigned to protein and nucleic acid features according to the extensive existing Raman literature.

There were two main goals of this work. One was to test the utility of Raman microscopy for following the workings of a large ∼400 kDa molecular machine. The second goal was to study the nucleotide incorporation reaction in single crystals of *Tth* RNAP by microscopy and, by combination of the data with time-resolved X-ray crystallographic analysis, to provide molecular details of the transcription elongation mechanism. The same approach has been successful in the study of β-lactamase−inhibitor reactions[13] as well as the transcription initiation reaction in enterobacteriophage (N4) RNA polymerase.[14−16] Although it was feasible to obtain Raman data from reactions in single crystals, unfortunately it was not yet possible to obtain high-resolution, atomic-level, X-ray structures from the TthEC crystals.

The Raman results show that the TthEC has been crystallized in two forms. In one, *GTP soaking into the crystals was incorporated into the nascent RNA chain quickly within minutes and with little detectable perturbation of the protein or nucleic acid conformations; this is described in our recent publication.[12] The crystal form described in the work presented here incorporated GMP from [^{13}C,^{15}N]GTP more slowly, in 1−2 h, following substantial changes in protein and nucleic acid conformation and/or orientation within the crystal. To understand the molecular-level differences in the two forms of the crystal, we must await advances that yield crystals diffracting X-rays at better than 3 Å resolution.

EXPERIMENTAL PROCEDURES

Collection of Raman Data of [^{13}C,^{15}N]GTP Soaking into the TthEC Crystal. Purification methods of the *Tth* RNAP core enzyme and crystallization of TthEC are as described previously.[17] Using a Raman microscope, Raman spectra from a single crystal (∼500 μm) of the TthEC are collected. The TthEC crystal is stabilized in a 5 μL hanging drop containing equilibrium buffer {EB [4% PEG 10000, 30% 1,6-hexanediol, 50 mM Tris (pH 8.5), and 10 mM magnesium acetate]} for 1 h before Raman spectra are collected. The hanging drop is placed on a siliconized cover slide, sealed in a well containing 1 mL of reservoir solution [3% PEG 10000, 30% 1,6-hexanediol, 50 mM Tris (pH 8.5), and 120 mM magnesium acetate], and held in a crystallization tray on the microscope stage. A krypton laser beam (647.1 nm) with a power of 120 mW is focused into the TthEC crystal. Under these conditions, the temperature of the crystal is increased to approximately 30−35 °C after being heated by the laser beam.[18] Crystal warming by the laser beam is essentially instantaneous, within the dead time of our Raman experiment. A microthermocouple shows a temperature rise to 30−35 °C within seconds,[18] after which equilibrium is reached and no further increase in temperature is detected. Each Raman spectrum is collected for 300 s (5 s × 60 accumulations) at known time points during the 3 h experiment using Holograms

DOI: 10.1021/acs.biochem.5b00484
Biochemistry 2015, 54, 5297−5305

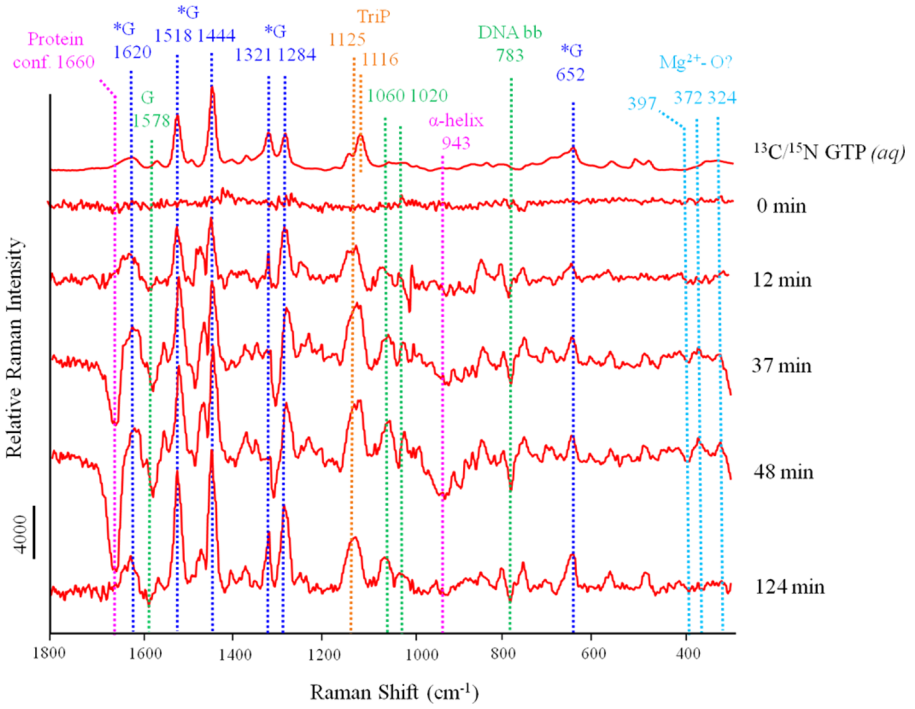

Figure 2. Stacked spectra of [^{13}C,^{15}N]GTP during diffusion into TthEC crystal. Monitoring the course of the *in crystallo* transcription elongation reaction of *Tth* RNAP via Raman difference spectroscopy. The reaction is tracked during the 3 h NTP "soak-in". Raman features of the substrate alone are represented in the top spectrum [50 mM aqueous [^{13}C/^{15}N]GTP (*GTP)]. The colored dotted lines highlight key features of the reaction, such as substrate *GTP soaking into the crystal; the blue dotted lines represent *G ring modes 1518, 1444, 1321, 1284, and 652 cm^{-1}. The triphosphate mode at 1125 cm^{-1} (orange) tracks the progress of the NTP incorporation reaction, while the mode at 1116 cm^{-1} represents the triphosphate of aqueous *GTP. Protein conformational changes are highlighted with pink dotted lines at 1660 and 943 cm^{-1}. They reach a maximal negative intensity at 48 min and decrease to zero by 110 min.

software (Kaiser Optical). In addition to the crystal spectrum, a spectrum of the surrounding equilibrium buffer (EB), in which the crystal is immersed, is also recorded. In short, the buffer spectrum is subtracted from the crystal spectrum to obtain a Raman difference spectrum of the "virgin" complex. Afterward, the TthEC crystal is transferred to a new 5 μL hanging drop containing a substrate (*GTP) soaking solution [4% PEG 10000, 30% 1,6-hexanediol, 50 mM Tris (pH 8.5), 10 mM magnesium acetate, and 2 mM *GTP]. Thus, the phosphodiester bond formation after *GTP and metal addition is monitored in the TthEC crystal that contains core *Tth* RNAP, a 9 bp DNA–RNA hybrid, a 19 bp DNA duplex, *GTP, and active site magnesium (Figure 1c). Again, a buffer spectrum surrounding the reactive TthEC crystal is subtracted from the Raman spectrum of the crystal at *x* min during the reaction. Finally, to reveal the state of the *GTP-bound TthEC, including protein and DNA structural changes as a function of time during RNA synthesis, a series of secondary subtractions of TthEC at *x* min *GTP soak-in minus "virgin" TthEC were calculated using the RNAP's phenylalanine ring feature at 1002 cm^{-1} as an internal intensity standard. A more thorough explanation detailing the Raman difference spectral calculations, Raman data analysis, and deriving kinetics from Raman spectroscopic data points are outlined in our initial study of TthEC.[12]

It should be noted that the overlap achieved in the spectral subtractions is superb, indicated by the quality of the Raman difference spectra. The signal-to-noise ratio is 190/1 (Figure S2) in the spectrum of the TthEC crystal when *GTP has been soaked for 48 min (before secondary subtraction of substrate-free TthEC). Also, the signal-to-noise ratio is 15/1 in the time-dependent Raman difference spectra of substrate-soaked TthEC crystals in Figure 2 and Figure S3. The final Raman difference spectra tend to be noisier because the intensity changes are <5% of the major bands in Figure S2. Although this limits the accuracy of the kinetic values derived from the standardized intensities of major marker bands, the kinetic data presented in Figure 3a–d semiquantitatively represent the trends in the various populations addressed. The kinetic plots in Figure 3a–d are obtained by measuring the height intensities of the respective Raman peak at each time point. These heights are all standardized by using an internal peak that is unchanging. Each height intensity is divided by the internal standard peak, such as the phenylalanine ring mode at 1002 cm^{-1} seen in Figure S2.

Raman Spectroscopic Assignments. A considerable aid in identifying key Raman marker bands in the Raman difference spectra comes from the use of *GTP, where guanosine is labeled with ^{13}C and ^{15}N. Thus, the isotopically labeled substrate can be distinguished from analogous bases in the nucleic acid scaffold (Figure 1c) crystal complex, which contains unlabeled guanosine, because the *G ring modes are typically shifted down 20–40 cm^{-1} in the Raman spectrum (Figure S1). In addition, assignments are buttressed by an extensive literature, as well as our earlier work on the *de novo* transcription initiation reaction of N4 virion RNAP.[14]

In an unforeseen aid to assignment, we have been able to utilize our Raman work on Mg^{2+} binding to ribozyme crystals.[19] In the latter, we identified Raman bands due to magnesium penta- or tetrahydrate binding to the negatively charged nonbridging oxygens in the phosphodiester linkages of the ribozyme's backbone. These occur in the 300–350 cm^{-1} region

DOI: 10.1021/acs.biochem.5b00484
Biochemistry 2015, 54, 5297–5305

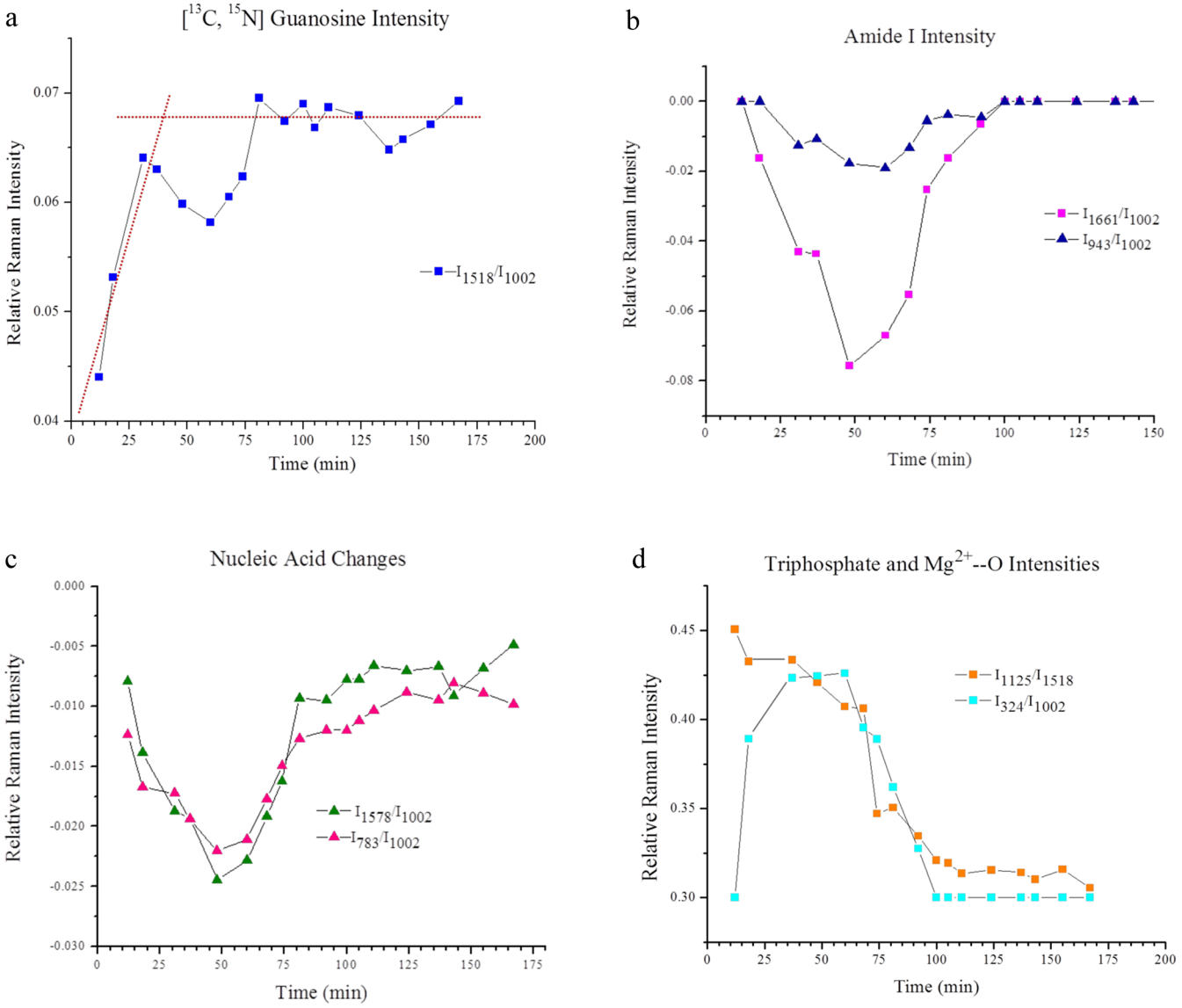

Figure 3. Raman height intensities of essential elongation reaction marker bands. (a) Guanosine ring mode at 1518 cm^{-1} as *GTP soaks into the crystal. It reaches the first maximum at approximately 20 min and continues until it maximizes to a second level at 85 min and plateaus. In the absence of a large protein conformational change, the intersection of the two lines represents the time point at which the beginning of the plateau takes place. (b) Amide I and α-helix height intensities. They reach a maximal decrease at 48 min *GTP soak-in and are reversible. (c) Dynamics of DNA-associated Raman marker bands. Peaks at 1578 and 783 cm^{-1} are assigned to unlabeled G and A ring modes and DNA backbone modes, respectively. All peak heights were standardized to the height of the phenylalanine mode at 1002 cm^{-1} in the mother spectrum, i.e., in the spectrum [TthEC at x min minus buffer near x minutes]. (d) Trend in triphosphate and Mg^{2+}−O time dependence. The height intensity of the triphosphate moiety of *GTP and magnesium-associated mode decrease during the course of the reaction. Catalysis begins around 65 min.

and are essentially Mg^{2+}−oxygen stretching modes. Remarkably, spectral features in this region from the reacting TthEC crystal appear and disappear with the same time dependence as chain elongation (see below). This raises the possibility that we are observing the assembly and disassembly of the bimagnesium active site. However, additional work is needed to confirm the assignment to Mg^{2+}−O vibrational modes.

RESULTS

Intracrystal Population of [^{13}C,^{15}N]GTP during Soak-In. Selected Raman difference spectra recorded as *GTP soaks into the TthEC crystal over the course of 2 h are shown in Figure 2; a complete data set is presented in Figure S3. The population of the ^{13}C- and ^{15}N-labeled guanosine (*G) moiety of *GTP within the crystal can be followed by its purine ring vibrational modes at 1518 and 652 cm^{-1} that appear in spectroscopic "windows" with minimal overlap from other signals. The *G modes near 1321 and 1284 cm^{-1} are less useful because Raman signals from polyethylene glycol in the buffer surrounding the crystal occur in this region and are difficult to subtract precisely in the difference trace. The intensities of the 1518 cm^{-1} Raman peaks from Figure 2 are plotted as a function of time in Figure 3a. These peaks are standardized using the peak height of the phenylalanine ring mode at 1002 cm^{-1} in the mother spectrum of the reacting crystal (before secondary subtraction of the substrate-free TthEC spectrum) at the data collection time indicated. Figure S2 depicts a mother spectrum used for standardization. In Figure 3a, the *G intensity continuously increases until 37 min, at which time it decreases until approximately 60 min and then rises again to a plateau

DOI: 10.1021/acs.biochem.5b00484
Biochemistry 2015, 54, 5297−5305

around 80 min. The dip in the *G base intensity at ∼75 min (Figure 3a) may be explained by a transient Raman dichroism (Figure S4). These are changes in the average orientation of the *G ring plane with respect to the direction of the laser beam between ∼30 and ∼90 min.

Protein and Nucleic Acid Conformational Changes Triggered by [^{13}C,^{15}N]GTP. A striking feature in Figure 2 is the negative band near 1660 cm^{-1}. According to its position and broad profile, this Raman peak can be assigned confidently to an amide I band with an additional conclusion, stemming from its position, that it contains substantial contributions from α-helix structures.[20] The latter finding is supported by the broad negative peak centered near 943 cm^{-1} that is known to originate from α-helix motions.[14,21] Figure 3b plots the standardized amide I intensities (1661 cm^{-1}, pink squares) and shows that its intensity change is reversible. The latter amide I/α-helix Raman mode reaches its maximum at 50 min, shortly after the *GTP population reaches a maximum and cannot be detected by 100 min (Figure 3b). The same reversible change is seen for the less intense 943 cm^{-1} α-helix feature (Figure 3b, blue triangles). The changes in amide I/α-helix intensity are significant and may be due to a reversible change in protein secondary structure. At its maximum at 48 min, the 1661 cm^{-1} intensity is approximately 2.7% of the amide I feature in the mother spectrum in Figure S2. In addition, some or all of the change in intensity can be due to a change in the orientation of α-helix structure, giving rise to Raman dichroism (Figure S4).

There are two classes of Raman probes that can monitor changes in nucleic acids during the elongation reaction. When purine and pyrimidine rings change their degree of base stacking, they often change their intensity due to Raman hypo- or hyperchromism. Additionally, a change in base orientation can affect its Raman intensity, due to Raman dichroism.[20,22,23] The negative peak near 1578 cm^{-1} in Figure 2 is due to changes in Raman intensities of unlabeled G and/or A ring modes on the DNA and/or RNA strands (both G and A have modes in the 1575−1580 cm^{-1} region; however, G displays a more intense mode), where they exhibit more intensity in the nonreacting crystal. Although we cannot identify which bases are changing their environments, the 1578 cm^{-1} negative band provides a general probe for nucleic acid conformational changes. It is notable that several unlabeled G bases are close to the *GTP insertion site (see the nucleic acid sequence in Figure 1c). Complementary information comes from the negative peak seen at 783 cm^{-1} in Figure 2. This reports on changes in the DNA backbone because the stretching vibration for the DNA's -C-O-P-O-C- phosphodiester groups occurs near 783 cm^{-1}.[24,25] Figure 3c plots the changes in intensities of G/A ring modes (mostly G), 1578 cm^{-1} (green triangles), and the phosphodiester backbone, 783 cm^{-1} (pink triangles), as a function of time. Strikingly, they show very similar behavior, with minima near 50 min and relaxation back to original values after 100 min.

Onset of Catalysis. An important *GTP feature is the mode near 1125 cm^{-1}; this is due to vibration(s) of the triphosphate tail (Figure S1a). Thus, it reports on the loss of *GTP population present as *GMP is incorporated. Figure 3d describes the intensity of the triphosphate band that is divided by the Phe ring mode at 1002 cm^{-1} (from the mother spectrum as an intensity standard). Figure 3d (orange squares) shows that the triphosphate intensity declines after ∼65 min and reaches a minimum at approximately 100 min, which is ∼65% of the intensity compared to the initial intensity for aqueous [^{13}C,^{15}N]GTP (Figure S1a). From this, we conclude that ∼35% of the *GTPs within the crystal has been incorporated into the RNA chain (hence the loss of triphosphate) and that the remaining 65% of the population is not covalently incorporated at the 3′-end of RNA. This second population can bind at one or more other sites on the enzyme, or in the crystal's solvent channels. We repeated this calculation using the *G ring mode at 1518 cm^{-1} as an internal standard. Measuring triphosphate mode/*G (1518 cm^{-1}) before and after catalysis showed that approximately 40% *GTP had been incorporated.

Another potentially informative, though less well characterized, region of the difference spectra is between 300 and 400 cm^{-1} (Figure 2). This contains peaks that "appear" and "disappear" on the 20−150 min time frame. The feature near 324 cm^{-1} is tentatively assigned to the formation of a Mg^{2+}−O^- mode from magnesium binding to an O^- atom. A similar species was first identified in ribozyme Raman studies.[19] As is seen in Figure 3d (cyan squares), its decay from the maximum at 50−60 min also follows the loss of *GTP population. We speculate that we may be observing the formation and dissolution of the Mg^{2+}−O^- contacts in the active site.

DISCUSSION

Conformational Changes in GTP, Protein, and Nucleic Acid. *GTP.* The curve seen in Figure 3a represents the trend in the guanosine ring mode height intensity as a function of time. The "dip" in the curve with the minimum at 50−60 min is ascribed to the large and reversible conformational changes in the enzyme complex that are also maximal at 50 min. The conformational change alters the orientation of the *G rings with respect to the fixed crystal axes, and thus the incoming laser beam, and reduces the Raman scattering. The latter phenomenon is termed Raman dichroism; on average, the plane of the *G rings becomes more parallel to the laser beam entering the crystal. Raman dichroism is explained in Figure S4. By drawing lines from the ascending and plateau regions on Figure 3a, we can take the point of intersection to be an approximation of the *GTP population kinetic trend in the absence of the *G ring plane reorientation. This procedure indicates that the *G intensity is approaching its maximum at ∼37 min soak-in and plateaus thereafter.

Protein. The negative peaks near 1660 and 943 cm^{-1} are due mainly to changes in α-helical content. The 1660 cm^{-1} peak is an amide I feature that has major contributions from α-helices, and the band at 943 cm^{-1} is another α-helix signature. The reversible intensity changes seen in the α-helix signatures during *GTP soak-in are due to a change in α-helix content in the reacting crystal compared to the "virgin" crystal at time zero. However, a second possible contribution may stem from Raman dichroism. A change in protein orientation with respect to the fixed crystal axes (and the fixed laser beam direction) is possibly reorienting a subunit in the crystal, resulting in lower Raman intensity averaged over all α-helices in the reacting enzyme because of the tensorial nature of Raman scattering. The dichroism seen in Raman scattering of biopolymers has been discussed in several publications,[22] and it is explained in detail in Figure S4. The issue of Raman dichroism is complicated further by the fact that there are varying orientations of the active site in the crystal. The TthEC crystals contain one RNAP−DNA−RNA complex per asymmetric unit (Protein Data Bank entry 2O5I),[2] and each unit cell has eight asymmetric units with different orientations.

DOI: 10.1021/acs.biochem.5b00484
Biochemistry 2015, 54, 5297−5305

Nucleic Acids. The nucleic acid marker band at 1578 cm^{-1} represents vibrations of unlabeled G ring modes in the nucleic acid sequences of the template DNA, nontemplate DNA, and RNA strands, while the 783 cm^{-1} feature is generally assigned to vibrational stretching modes of the C-O-P-O-C DNA backbone. Interestingly, two other marker bands that could possibly be assigned to the nucleic acid backbone follow the same time course as the 1578 and 783 cm^{-1} modes. These modes at 1060 and 1020 cm^{-1} (Figure S5) may be attributed to contributions from the distorted nucleic acid backbone that have not been previously discussed in the Raman literature. This is a topic for future research.

All three changes in *GTP, protein, and nucleic acid are summarized in a schematic in Figure 4. First, *GTP soaks into the crystal and reaches a stable population around 37 min. Second, the maximal protein and nucleic acid changes occur shortly after *GTP is fully soaked. The kinetic trends of protein and nucleic acid conformational changes simultaneously reach a maximum at 50 min; however, they begin to reverse just before catalysis begins. Subsequently, catalysis is initiated after 60−70 min. Although, for the sake of simplicity, the protein and nucleic acid changes are shown in the positive direction in Figure 4, the experimental Raman intensity changes are negative in the difference spectra (Figure 2 and Figure S3).

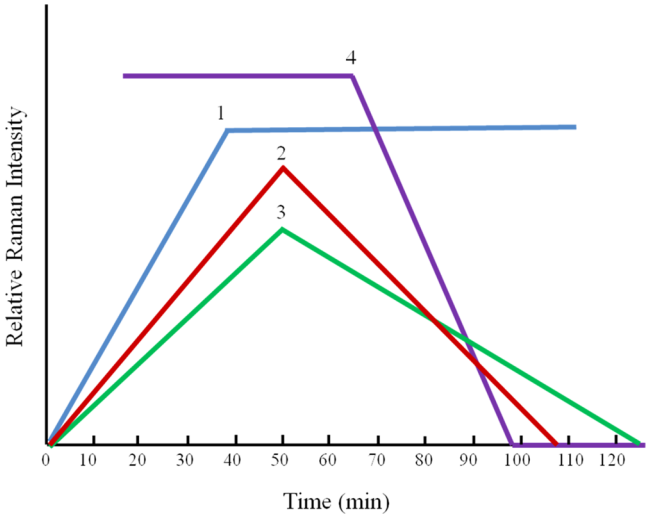

Figure 4. Schematic representation of *in crystallo* kinetics obtained from Raman experimentation, durinh which [^{13}C,^{15}N]GTP (*GTP) was soaked into a TthEC crystal. (1) *G (ring mode at 1518 cm^{-1}) soaks into the crystal. (2) The protein conformational change is maximal (amide I, 1660 cm^{-1}). (3) DNA perturbation is maximal (backbone mode, 783 cm^{-1}). (4) Catalysis begins (decline in the triphosphate Raman mode at 1125 cm^{-1}). Plots 2 and 3 show negative changes in intensity; however, the modulus is plotted here.

Possible Explanations for Slow *in Crystallo* Kinetics. In comparison to our recently published work on TthEC,[12] in which the kinetics of GTP incorporation within a crystal are rapid on the time scale of minutes, the results for the crystal presented here exhibit slower crystallographic kinetics on the time scale of tens of minutes. In our previous work, pyrophosphorolysis experiments confirmed that the TthEC was in the post-translocated state.[12] However, for the particular crystal tray yielding the crystal described here, it is possible that the TthEC crystals may have been crystallized in the pretranslocated state (although similar crystallization conditions were used as previously described[12]). Beginning in the pretranslocated state may explain the present Raman kinetic data reported here because significant protein conformational changes are observed to occur in the crystal before the onset of catalysis. With the TthEC starting in the pretranslocated state, the enzyme must undergo major conformational changes in α-helical structure and orientation.[3] According to the nucleotide addition cycle model proposed by Vassylyev et al., a change in α-helical content is associated with the interconversion between translocation states.[3] This may explain the reversibility of α-helical intensity at 48 min (Figure 2, Figure S3, and Figure 3b) and why catalysis occurs following translocation. It may also be possible that the large conformational changes observed are attributed to *GTP driving translocation from the pre- to post-translocated state.[26] The dip in *GTP ring mode intensity in Figure 3a may be explained by the reorientation of the *G ring as it drives translocation, with the *G rings, on average, becoming more parallel to the plane of the incoming laser beam as translocation occurs.

An alternative explanation for the slower kinetics observed with the present TthEC crystal compared to the in *crystallo* kinetics reported previously[12] may be the consequences of a TthEC crystal that was grown in an alternately packed conformational state, giving rise to the phenomenon of transcriptional pausing. It is possible that an altered crystal packing or a varied *in crystallo* conformation may have led to a misalignment of the 3′-OH group on the nascent RNA in the active site.[27] The latter situation would induce transcriptional pausing, causing the active site to reorient itself for optimal alignment for catalysis to occur.[28] The conformational changes thus observed may be related to reorientation of the active site. If it is assumed that the EC begins in the post-translocated state (as demonstrated in previous work[12]), the slow NTP binding, protein, and nucleic acid conformational changes as well as retarded catalysis may be attributed to a transcriptionally paused complex. According to Neuman and colleagues, RNAP transcribes DNA discontinuously with periods of rapid nucleotide addition punctuated by frequent pauses.[29] Single-molecule studies using 1 mM NTP showed that pauses are transient, lasting anywhere from 1 to 6 s at 21 °C in solution. It must be noted that the TthEC crystal reported here was uniquely large (~500 μm) compared to the TthEC crystals (~100 μm) used in our recently reported Raman and PAGE data.[12] The crystal size may play a role in explaining the disparity between rapid and slow Raman crystal kinetics because a low NTP concentration (1−2 mM used during Raman experiments) has been known to induce transcriptional pausing.[29] Therefore, 1−2 mM substrate [^{13}C,^{15}N]GTP may possibly have a pausing effect on a large crystal versus a smaller crystal. However, it is difficult to reconcile the reversible nature of the experimental kinetic data with a pause-type explanation.

It is also interesting to note that there is evidence of an additional population(s) of *GTP in the crystal that represents 1.5−2 times the active site population that is being incorporated as reported also by Antonopoulos et al.[12] In earlier work, such as in single-molecule studies of *Escherichia coli* RNAP[30] and X-ray crystallographic work on Pol II,[31,32] the possibility of secondary NTP binding sites such as the nontemplated "E site" or ancillary templated NTP binding to downstream DNA[33−36] has been discussed. In the future, X-ray crystallographic studies of the TthEC system are needed to search for a possible location for the second population.

DOI: 10.1021/acs.biochem.5b00484
Biochemistry 2015, 54, 5297−5305

A potentially crucial observation is the formation and dissolution of the bands in the 300−400 cm^{-1} region (Figures 2 and 3d) that we ascribe to the formation and dissolution of the functional active site containing two Mg^{2+} ions. In our previous work where the reaction is faster,[12] we did not detect features in the Raman difference spectra between 300 and 400 cm^{-1}. This observation suggests that the active site is preformed and contains two Mg^{2+} ions, permitting the reaction to occur quickly, whereas in the work presented here, the active site is only completed by the GTP carrying in the second Mg^{2+} ion. This could, at least in part, explain the slower kinetics. Although every effort was made to reproduce the crystallization conditions, the Raman data suggest that the crystals used in the work presented here contained less Mg^{2+}. Future crystallization trials using a lower concentration of Mg^{2+} may determine if this leads to a different crystal form.

CONCLUSION

This work is part of a series of studies in which we have attempted to combine Raman microscopy and X-ray crystallography to define reaction pathways in crystals containing enzyme complexes. It was successful for characterizing drug compounds reacting with β-lactamases[13,37] and the transcription initiation step in the N4 virion RNA polymerase.[14,15] In both cases, the kinetics discovered by spectroscopy were used by the crystallographers to define the soak-in conditions to trap mechanistically vital enzyme intermediates. In the example presented here, we had planned to combine Raman and X-ray studies to provide details of the RNA elongation reaction pathways in crystals of the RNA polymerase from *T. thermophilus*. Because of its size (∼400 kDa) and complexity, this provided an unprecedented challenge for Raman analysis. In our crystallization trials, we identified two crystal forms, one of which incorporated NTP very quickly on the time scale of minutes and is described in a recent publication.[12] The second, the topic of this paper, undergoes complex conformational changes on the time scale of tens of minutes. Unfortunately, thus far it has not been possible to obtain detailed atomic-level resolution from crystals of the TthEC (unpublished work, K. Murakami). Thus, we can present only the results obtained by Raman microscopy. We have observed conformational changes in other polymerases occurring in tens of minutes.[14,38] However, the Raman results presented here are unprecedented because this is the first time such a clear progression of conformational changes has been observed. When the cognate nucleotide GTP is soaked into a crystal of the TthEC catalytic complex, reversible changes are seen over the time course of 10−100 min for both protein and nucleic acid components of the crystal. These reach a maximum at approximately 50 min. Incorporation of GMP from the GTP starts at ∼60 min and is complete by 100 min.

These results contrast sharply with those from the other form of the crystal grown from the TthEC, where incorporation of GTP occurs in a few minutes and little change is seen in nucleic acid or protein conformations.[12] We propose two possible explanations for the slow kinetics; one is that the TthEC has been crystallized in the pretranslocated state, and thus we are observing the conformational changes associated with translocation to the post-translocated state prior to catalysis occurring. Alternatively, we may have crystallized the sample in a transcriptionally paused state that must undergo conformational changes to bring the active site into the conformation favored for catalysis to occur. Although we cannot form a definitive conclusion for the slow kinetics, these results demonstrate that the Raman data can detect new and unexpected forms of the EC in the crystal. Detailed X-ray crystallographic studies are needed to resolve this issue; however, these must await the discovery of EC crystals of *T. thermophilus* that diffract to high atomic resolution.

Thus far, it is always true for the reactions we have studied *in crystallo* that the kinetics are much slower than for the same reaction in solution. For example, for the relatively simple β-lactamase SHV-1 reacting with a mechanism-based inhibitor tazobactam, reaction intermediates have a lifetime in the crystal $>10^3$ times longer than in solution.[39] For both the TthEC crystals discussed in our previous manuscript[12] and in the work presented here, chain elongation is slowed by many thousand-fold compared to that in solution or *in vivo*. There are several possible reasons for this; as Geremia et al. discuss, times for diffusion of small molecules into crystals depend on ligand size, crystal shape, and accessible volume.[40] In the crystals presented here, access to the active site may be restricted by partially blocked solvent channels. Importantly, segments of enzymes have to move to perform the chemistry of catalysis, and this movement may be severely constrained by protein−protein contacts in the crystal. This is especially critical for large molecular machines like *Tth* RNAP. *In vivo* chain elongation occurs in 0.01−0.1 s. In the TthEC crystal discussed here, the reaction takes about 1 h, 30000 times slower than in solution.

ASSOCIATED CONTENT

Supporting Information

The Supporting Information is available free of charge on the ACS Publications website at DOI: 10.1021/acs.biochem.5b00484.

Raman spectra of labeled and unlabeled GTP, Raman "mother" spectrum of the *T. thermophilus* elongation complex with [^{13}C,^{15}N]GTP before secondary subtraction, complete series of Raman spectra for *GTP soak-in, a schematic explanation of Raman dichroism, and kinetic dynamics of two new spectroscopic features hypothesized to be DNA-associated Raman marker bands (PDF)

AUTHOR INFORMATION

Corresponding Author

*E-mail: prc5@case.edu.

Present Address

§B.A.W.: Janssen Research & Development, LLC, Spring House, PA 19477.

Funding

This work was supported by National Institute of General Medical Sciences Grant R01 GM54072 (to P.R.C.).

Notes

The authors declare no competing financial interest.

ACKNOWLEDGMENTS

We thank Dr. Kastuhiko S. Murakami at Pennsylvania State University for providing purified *T. thermophilus* protein as well as nucleic acid templates. We are also indebted to the reviewer who suggested a comparative analysis of the 300−400 cm^{-1} regions of the Raman spectra of the "fast" and "slow" forms of the TthEC crystals.

DOI: 10.1021/acs.biochem.5b00484
Biochemistry 2015, 54, 5297−5305

REFERENCES

(1) Bochner, B. R., and Ames, B. N. (1982) Complete analysis of cellular nucleotides by two-dimensional thin-layer chromatography. *J. Biol. Chem. 257*, 9759−9769.

(2) Vassylyev, D. G., Vassylyeva, M. N., Perederina, A., Tahirov, T. H., and Artsimovitch, I. (2007) Structural basis for transcription elongation by bacterial RNA polymerase. *Nature 448*, 157−162.

(3) Vassylyev, D. G., Vassylyeva, M. N., Zhang, J., Palangat, M., Artsimovitch, I., and Landick, R. (2007) Structural basis for substrate loading in bacterial RNA polymerase. *Nature 448*, 163−168.

(4) Zhang, G. Y., Campbell, E. A., Minakhin, L., Richter, C., Severinov, K., and Darst, S. A. (1999) Crystal structure of Thermus aquaticus core RNA polymerase at 3.3 angstrom resolution. *Cell 98*, 811−824.

(5) Cramer, P., Bushnell, D. A., and Kornberg, R. D. (2001) Structural basis of transcription: RNA polymerase II at 2.8 angstrom resolution. *Science 292*, 1863−1876.

(6) Gnatt, A. L., Cramer, P., Fu, J. H., Bushnell, D. A., and Kornberg, R. D. (2001) Structural basis of transcription: An RNA polymerase II elongation complex at 3.3 angstrom resolution. *Science 292*, 1876−1882.

(7) Darst, S. A., Polyakov, A., Richter, C., and Zhang, G. Y. (1998) Insights into Escherichia coli RNA polymerase structure from a combination of x-ray and electron crystallography. *J. Struct. Biol. 124*, 115−122.

(8) Cheetham, G. M., and Steitz, T. A. (1999) Structure of a transcribing T7 RNA polymerase initiation complex. *Science 286*, 2305−2309.

(9) Yin, Y. W., and Steitz, T. A. (2002) Structural basis for the transition from initiation to elongation transcription in T7 RNA polymerase. *Science 298*, 1387−1395.

(10) Murakami, K. S., Masuda, S., Campbell, E. A., Muzzin, O., and Darst, S. A. (2002) Structural basis of transcription initiation: An RNA polymerase holoenzyme-DNA complex. *Science 296*, 1285−1290.

(11) Zhang, J., and Landick, R. (2009) Substrate Loading, Nucleotide Addition, and Translocation by RNA Polymerase. In *RNA Polymerases as Molecular Motors* (Buc, H., and Strick, T., Eds.) pp 206−229, RSC Biomolecular Sciences, Cambridge, U.K.

(12) Antonopoulos, I. H., Murayama, Y., Warner, B. A., Sekine, S.-i., Yokoyama, S., and Carey, P. R. (2015) Time-resolved Raman and polyacrylamide gel electrophoresis observations of nucleotide incorporation and misincorporation in RNA within a bacterial RNA polymerase crystal. *Biochemistry 54*, 652−665.

(13) Helfand, M. S., Totir, M. A., Carey, M. P., Hujer, A. M., Bonomo, R. A., and Carey, P. R. (2003) Following the reactions of mechanism-based inhibitors with beta-lactamase by Raman crystallography. *Biochemistry 42*, 13386−13392.

(14) Chen, Y., Basu, R., Gleghorn, M. L., Murakami, K. S., and Carey, P. R. (2011) Time-resolved events on the reaction pathway of transcript initiation by a single-subunit RNA polymerase: Raman crystallographic evidence. *J. Am. Chem. Soc. 133*, 12544−12555.

(15) Basu, R. S., and Murakami, K. S. (2013) Watching the bacteriophage N4 RNA polymerase transcription by time-dependent soak-trigger-freeze X-ray crystallography. *J. Biol. Chem. 288*, 3305−3311.

(16) Gleghorn, M. L., Davydova, E. K., Basu, R., Rothman-Denes, L. B., and Murakami, K. S. (2011) X-ray crystal structures elucidate the nucleotidyl transfer reaction of transcript initiation using two nucleotides. *Proc. Natl. Acad. Sci. U. S. A. 108*, 3566−3571.

(17) Warner, B. (2012) Structural Study of Bacterial RNA Polymerase Conformational Changes During Transcription Elongation. Ph.D. Thesis, Pennsylvania State University, State College, PA.

(18) Carey, P. R. (2006) Raman crystallography and other biochemical applications of Raman microscopy. *Annu. Rev. Phys. Chem. 57*, 527−554.

(19) Gong, B., Chen, Y., Christian, E. L., Chen, J. H., Chase, E., Chadalavada, D. M., Yajima, R., Golden, B. L., Bevilacqua, P. C., and Carey, P. R. (2008) Detection of innersphere interactions between magnesium hydrate and the phosphate backbone of the HDV ribozyme using Raman crystallography. *J. Am. Chem. Soc. 130*, 9670−9672.

(20) Carey, P. R. (1982) *Biochemical Applications of Raman and Resonance Raman Spectroscopies*, Academic Press, New York.

(21) Pezolet, M., Pigeon, M., Menard, D., and Caille, J. P. (1988) Raman spectroscopy of cytoplasmic muscle fiber proteins - Orientational order. *Biophys. J. 53*, 319−325.

(22) Tsuboi, M., and Thomas, G. J. (1997) Raman scattering tensors in biological molecules and their assemblies. *Appl. Spectrosc. Rev. 32*, 263−299.

(23) Altose, M. D., Zheng, Y. G., Dong, J., Palfey, B. A., and Carey, P. R. (2001) Comparing protein-ligand interactions in solution and single crystals by Raman spectroscopy. *Proc. Natl. Acad. Sci. U. S. A. 98*, 3006−3011.

(24) Thomas, G. J., Benevides, J. M., Overman, S. A., Ueda, T., Ushizawa, K., Saitoh, M., and Tsuboi, M. (1995) Polarized Raman spectra of oriented fibers of A-DNA and B-DNA - Anisotropic and isotropic local Raman tensors of base and backbone vibrations. *Biophys. J. 68*, 1073−1088.

(25) Deng, H., Bloomfield, V. A., Benevides, J. M., and Thomas, G. J. (1999) Dependence of the raman signature of genomic B-DNA on nucleotide base sequence. *Biopolymers 50*, 656−666.

(26) Burton, Z. F., Feig, M., Gong, X. Q., Zhang, C. F., Nedialkov, Y. A., and Xiong, Y. L. (2005) NTP-driven translocation and regulation of downstream template opening by multi-subunit RNA polymerases. *Biochem. Cell Biol. 83*, 486−496.

(27) Kireeva, M. L., and Kashlev, M. (2009) Mechanism of sequence-specific pausing of bacterial RNA polymerase. *Proc. Natl. Acad. Sci. U. S. A. 106*, 8900−8905.

(28) Landick, R. (2009) Transcriptional pausing without backtracking. *Proc. Natl. Acad. Sci. U. S. A. 106*, 8797−8798.

(29) Neuman, K. C., Abbondanzieri, E. A., Landick, R., Gelles, J., and Block, S. M. (2003) Ubiquitous transcriptional pausing is independent of RNA polymerase backtracking. *Cell 115*, 437−447.

(30) Abbondanzieri, E. A., Greenleaf, W. J., Shaevitz, J. W., Landick, R., and Block, S. M. (2005) Direct observation of base-pair stepping by RNA polymerase. *Nature 438*, 460−465.

(31) Westover, K. D., Bushnell, D. A., and Kornberg, R. D. (2004) Structural basis of transcription: Separation of RNA from DNA by RNA polymerase II. *Science 303*, 1014−1016.

(32) Temiakov, D., Zenkin, N., Vassylyeva, M. N., Perederina, A., Tahirov, T. H., Kashkina, E., Savkina, M., Zorov, S., Nikiforov, V., Igarashi, N., Matsugaki, N., Wakatsuki, S., Severinov, K., and Vassylyev, D. G. (2005) Structural basis of transcription inhibition by antibiotic streptolydigin. *Mol. Cell 19*, 655−666.

(33) Zhang, C. F., and Burton, Z. F. (2004) Transcription factors IIF and US and nucleoside triphosphate substrates as dynamic probes of the human RNA polymerase II mechanism. *J. Mol. Biol. 342*, 1085−1099.

(34) Gong, X. Q., Zhang, C. F., Feig, M., and Burton, Z. F. (2005) Dynamic error correction and regulation of downstream bubble opening by human RNA polymerase II. *Mol. Cell 18*, 461−470.

(35) Holmes, S. F., and Erie, D. A. (2003) Downstream DNA sequence effects on transcription elongation - Allosteric binding of nucleoside triphosphates facilitates translocation via a ratchet motion. *J. Biol. Chem. 278*, 35597−35608.

(36) Batada, N. N., Westover, K. D., Bushnell, D. A., Levitt, M., and Kornberg, R. D. (2004) Diffusion of nucleoside triphosphates and role of the entry site to the RNA polymerase II active center. *Proc. Natl. Acad. Sci. U. S. A. 101*, 17361−17364.

(37) Padayatti, P. S., Helfand, M. S., Totir, M. A., Carey, M. P., Hujer, A. M., Carey, P. R., Bonomo, R. A., and van den Akker, F. (2004) Tazobactam forms a stoichiometric trans-enamine intermediate in the E166A variant of SHV-1 beta-lactamase: 1.63 angstrom crystal structure. *Biochemistry 43*, 843−848.

(38) Espinoza-Herrera, S. J., Gaur, V., Suo, Z., and Carey, P. R. (2013) Following DNA Chain Extension and Protein Conformational Changes in Crystals of a Y-Family DNA Polymerase via Raman Crystallography. *Biochemistry 52*, 4881−4890.

DOI: 10.1021/acs.biochem.5b00484
Biochemistry 2015, 54, 5297−5305

(39) Heidari Torkabadi, H. H., Che, T., Shou, J., Shanmugam, S., Crowder, M. W., Bonomo, R. A., Pusztai-Carey, M., and Carey, P. R. (2013) Raman Spectra of Interchanging beta-Lactamase Inhibitor Intermediates on the Millisecond Time Scale. *J. Am. Chem. Soc. 135*, 2895−2898.
(40) Geremia, S., Campagnolo, M., Demitri, N., and Johnson, L. N. (2006) Simulation of diffusion time of small molecules in protein crystals. *Structure 14*, 393−400.

DOI: 10.1021/acs.biochem.5b00484
Biochemistry 2015, 54, 5297−5305